Kinetic Range Spectral Features of Cross Helicity Using the Magnetospheric Multiscale Spacecraft

Tulasi N. Parashar, Alexandros Chasapis, Riddhi Bandyopadhyay, Rohit Chhiber, W. H. Matthaeus, B. Maruca, M. A. Shay, J. L. Burch, T. E. Moore, B. L. Giles, D. J. Gershman, C. J. Pollock, R. B. Torbert, C. T. Russell, R. J. Strangeway, and Vadim Roytershteyn

Phys. Rev. Lett. **121**, 265101 — Published 26 December 2018

DOI: 10.1103/PhysRevLett.121.265101

Kinetic range spectral features of cross-helicity using MMS Observations

Tulasi N. Parashar, Alexandros Chasapis, Riddhi Bandyopadhyay,
Rohit Chhiber, W. H. Matthaeus, B. Maruca, M. A. Shay
Department of Physics and Astronomy, University of Delaware, Newark, DE 19716, USA

J. L. Burch
Southwest Research Institute, San Antonio, TX, USA

T. E. Moore, B. L. Giles, and D. J. Gershman
NASA Goddard Space Flight Center, Greenbelt, MD, USA

C. J. Pollock
Denali Scientific, Fairbanks, Alaska, USA

R. B. Torbert
University of New Hampshire, Durham, NH, USA

C. T. Russell and R. J. Strangeway
University of California, Los Angeles, CA, USA

Vadim Roytershteyn
Space Science Institute, Boulder, CO, USA
(Dated: October 22, 2018)

We study spectral features of ion velocity and magnetic field correlations **in the magnetosheath (MS) and in the solar wind (SW)** using data from the Magnetospheric Multi-Scale (MMS) spacecraft. High resolution MMS observations enable the study of transition of these correlations between their magnetofluid character at larger scales into the sub-proton kinetic range, previously unstudied in spacecraft data. Cross-helicity, angular alignment and energy partitioning is examined over a suitable range of scales, employing measurements based on the Taylor frozen-in approximation as well as direct two-spacecraft correlation measurements. The results demonstrate signatures of alignment at large scales. As kinetic scales are approached, the alignment between $\mathbf{v}$ and $\mathbf{b}$ is destroyed by demagnetization of protons.

Introduction Turbulence is a ubiquitous feature of astrophysical plasma flows. Interplanetary spacecraft observations have been used to study various aspects of plasma turbulence over the last few decades including the systematic appearance of correlations of several types between fluctuations of the plasma velocity and the fluctuations of the magnetic field (e.g. [1–7] and many references therein). Such correlations are widely regarded as signatures of magnetohydrodynamic (MHD) fluctuations **and are an essential consideration in turbulence theories (e.g. [8–14])**. Here we employ the unique observational capabilities of the Magnetospheric Multi-Scale (MMS) Mission to examine these hitherto inaccessible correlations at kinetic sub-proton scales.

One of the features of MHD turbulence is the conservation of cross helicity [15]. The normalized cross helicity is defined as

$$\sigma_c = \langle |\delta z^+|^2 - |\delta z^-|^2 \rangle / \langle |\delta z^+|^2 + |\delta z^-|^2 \rangle \qquad (1)$$

where $\delta \mathbf{z}^{\pm} = \delta \mathbf{b}/\sqrt{\mu_0 m_i n_i} \pm \delta \mathbf{v}_p$; $\delta \mathbf{b}$ is the increment of magnetic field fluctuation $\mathbf{b}(\mathbf{x}) - \mathbf{b}(\mathbf{x}+\mathbf{r})$, written in Alfvén speed units as suggested by this definition, where $\mathbf{r}$ is a lag, n_i is the proton density, and $\mathbf{v}_p$ is the proton fluid velocity fluctuation (mean removed), and the brackets indicate a suitable volume average. σ_c is sensitive to both the relative alignment of the velocity and magnetic fluctuations, and their degree of energy equipartition. For an "Alfvénic" state the magnitude of cross helicity is very close to the value for Alfvén waves (~ 1). A lower value suggests a non-Alfvénic state. The importance of the ideal incompressible invariant cross helicity $\langle |z^+|^2 - |z^-|^2 \rangle$ in selecting equilibria was noted early on by Chandrasekhar [16] and Woltjer [17]. Later, in the context of MHD turbulence theory [18–20] it was noted that relaxation of energy in both 2 and 3-dimensions can lead to states that tend toward *point-wise* geometrical alignment, but not necessarily equipartition, of $\mathbf{v}$ and $\mathbf{b}$. Simulations subsequently showed that this tendency occurs rapidly and locally [21–24]. Subsequent research exploited the tendency for alignment of v & b fluctuations to estimate the degree of suppression of nonlinearity, thus influencing the slope of the turbulent spectrum [13, 14, 25, 26]. **See [4, 7, 27, 28] for detailed comparisons of observations to various theoretical models of turbulence in the MHD range.**

The situation becomes more complex as proton kinetic scales are approached, and non-MHD ef-

fects become important. The concept of helicity needs to be generalized as kinetic approximations, e.g. Hall physics [29], Hall & electron inertia [30], gyrofluid closure [31], and electron MHD [32] etc., are retained. This is a diverse set of closures, but one common feature is the breakdown of the MHD invariants as kinetic effects are retained. To the best of our knowledge this has not been demonstrated in observational studies, probably due to the lack of high time-cadence plasma data prior to MMS. We fill this gap by studying the scale-dependent breakdown of MHD concepts of alignment. A computation of the generalized helicities is beyond the present capabilities given the difficulties in measuring quantities such as vorticity in observational data.

The residual energy (difference of energy density in flow fluctuations and magnetic fluctuations) is related in MHD to the alignment issue both kinematically and dynamically. The normalized residual energy, $\sigma_r = (\delta\mathbf{v}^2 - \delta\mathbf{b}^2)/(\delta\mathbf{v}^2 + \delta\mathbf{b}^2)$ obeys an exact kinematic relation involving the alignment cosine: $\cos(\theta) \equiv (\delta\mathbf{v} \cdot \delta\mathbf{b})/\sqrt{|\delta\mathbf{v}||\delta\mathbf{b}|} = \sigma_c/\sqrt{1-\sigma_r^2}$. This relationship holds point-wise and for averages. Even prior to invoking turbulence theory, one sees readily, for a pure non-dispersive Alfvén wave packet, that one necessarily has $\sigma_c = 1$, $\cos(\theta) = \pm 1$, and $\sigma_r = 0$. **There is evidence that large scale properties of plasma might control the signatures of alignment and magnetic helicity close to the end of the inertial range [33].** Various turbulence theories pertain to the behavior of **the alignment** angle, and to the residual energy, in MHD and in the inertial range [19, 23, 25]. To the best of our knowledge no theory exists that describes alignment in the kinetic range where the MHD approximation breaks down.

Here we use burst-mode data from the MMS spacecraft to provide a novel view of cross helicity, alignment and residual energy in the **magnetosheath (MS) as well as the solar wind (SW)**, exploiting MMS time-resolution and the multi-spacecraft observations to probe these quantities in the kinetic range.

Data: We use data from the four spacecraft MMS mission, which emphasizes high cadence observations of magnetic reconnection [34, 35]. The magnetic field data are obtained from the Fluxgate Magnetometer (FGM) [36], providing 128 samples per second. The plasma moments used here are taken from the Fast Plasma Instrument (FPI) [37], providing proton moments at 15 samples per second, and electron moments at 30 samples per second. The four MMS spacecraft maneuver in a tetrahedral formation, varying the inter-spacecraft separation over a wide range of distances. The spacecraft separation during the intervals employed here lies below proton inertial length $d_i = c/\omega_{pi}$, where c is the speed of light and ω_{pi} is the proton plasma frequency. We study two intervals: **i)** A 40 minute long magnetosheath interval from 2017-12-26 starting at 06 : 12 : 43 UTC. **The spacecraft were at roughly 14.8** R_E**,** $V_p \sim 238$ **km/s,** $n \sim 22$ **cm**$^{-3}$**, and** $\beta_p \sim 4.49$**. ii)** An hour long interval in the solar wind from 2017-11-24 starting at 01 : 10 : 03 UTC. **The spacecraft were at roughly 24.9** R_E**,** $V_{sw} \sim 377$ **km/s,** $n \sim 8.6$ **cm**$^{-3}$**, and** $\beta_p \sim 1.3$**. The FPI solar wind data were pre-processed using a spectral Hampel filter as described in detail in Bandyopadhyay et al. [38].**

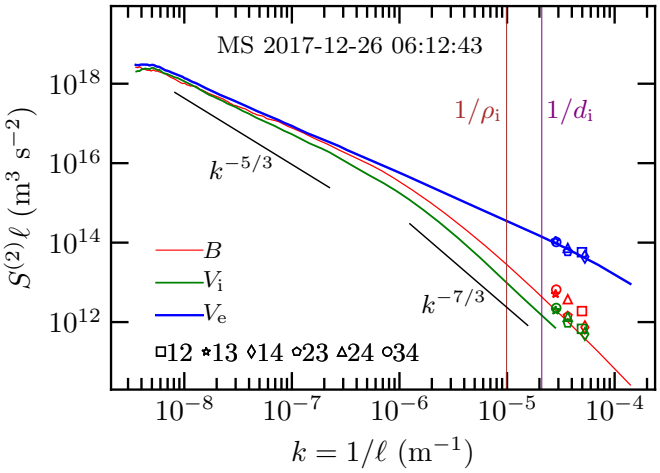

FIG. 1: Equivalent spectra for B, V_i, V_e. Lines are single spacecraft values using Taylor's hypothesis, symbols are multi-spacecraft estimates.

Results: We begin by studying the spectral features of magnetic field and flows. To leverage the advantages afforded by multi-spacecraft observations we compute the equivalent spectra using the structure function technique as described in [39]. The second-order structure function of a vector (e.g. magnetic field) is defined as

$$D_b^{(2)}(\mathbf{r}) \equiv \left\langle |\mathbf{b}(\mathbf{x}+\mathbf{r}) - \mathbf{b}(\mathbf{x})|^2 \right\rangle \tag{2}$$

With this definition of $D_b^{(2)}$, $S^{(2)}(\lambda) \equiv D^{(2)}(\lambda) \cdot \lambda$ behaves like an "equivalent spectrum" as a function of an effective wavenumber $k \equiv 1/\lambda$.

Structure functions from a single spacecraft use the Taylor hypothesis to transform time lags into spatial lags, i.e., $\lambda = V\tau$ where V is the mean flow speed and τ the time lag. Multi-spacecraft observations enable the direct computation of structure function at a particular physical lag λ defined by the spacecraft separation, using time averaging to attain statistical significance. The four MMS spacecraft correspond to six different physical lags without resorting to Taylor's hypothesis. Given the small separation of the MMS spacecraft, the directly computed two-point structure functions can be compared with the single-spacecraft Taylor hypothesis results at scales well into the kinetic range.

Figure 1 shows the equivalent spectra for the magnetic field, proton velocity, and electron velocity for the

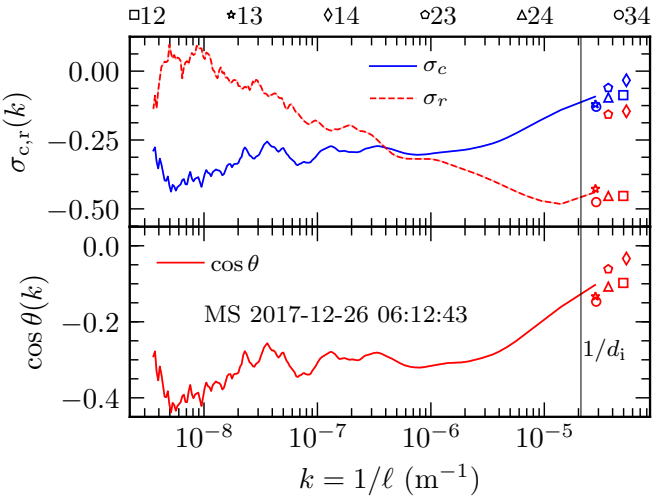

FIG. 2: Magnetosheath equivalent spectra of (top panel) σ_c and σ_r, and (bottom panel) the alignment cosines. Lines are single spacecraft estimates using Taylor's hypothesis and symbols are multi-spacecraft estimates.

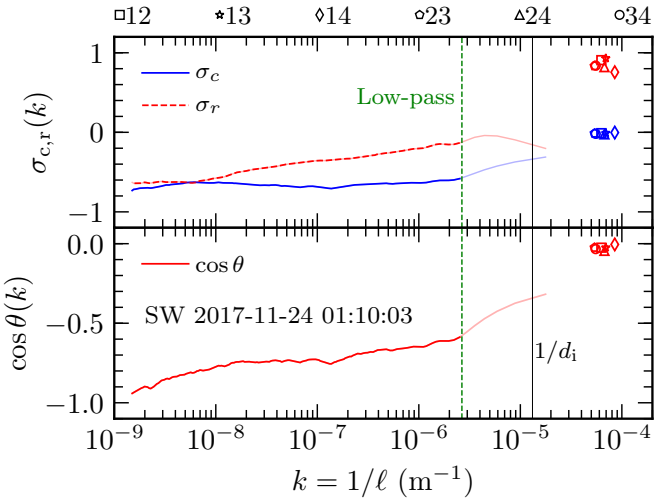

FIG. 3: Solar wind equivalent spectra for σ_c, σ_r, and alignment cosines.

magnetosheath interval of interest. As above, the magnetic field has been converted to Alfvénic units to make direct comparisons with proton and electron velocities. In the inertial range the magnetic field and the proton and electron velocities have similar power. However, they begin to depart from one another at scales almost a decade larger than d_i. In the kinetic range the multi-spacecraft observations match extremely well with the single-spacecraft observations computed using Taylor's hypothesis. This indicates that Taylor's hypothesis is applicable even in the kinetic range at least to scales slightly below the ion inertial length, consistent with earlier reports [39]. The distances between spacecraft were spread over a moderate range (18.9-35.41 km) and the multi-spacecraft values follow the single-spacecraft curve through this range. The slight mismatch of single-spacecraft and multi-spacecraft values for protons is likely due to noise in proton measurements.

Having compared the single-spacecraft and multi-spacecraft observations for the familiar spectra of the magnetic field and proton velocity, we now proceed to compute the cross helicity spectrum using the structure function technique described above. First the equivalent spectra of $z^{\pm}$ are computed and Equation 1 is used to compute the equivalent spectrum of cross helicity.

The top panel of figure 2 shows the equivalent spectrum for cross helicity, computed from the Elsasser variables, for the magnetosheath interval. The figure also shows the estimates of cross helicity at sub-proton lags computed using multi-spacecraft lags. At larger scales the interval has a cross helicity of -0.3 and it approaches 0 as we approach smaller scales. Multi-spacecraft values not only match the single-spacecraft estimate, they continue the single-spacecraft trend. The decrease in cross helicity with decreasing lag indicates that the alignment between flow and magnetic field decreases as kinetic scales are approached. The decrease in cross helicity begins at about the scales where electron and proton spectra depart from each other ($k\ell \sim 10^{-6}$), hence this decrease is likely a direct result of break-down of the MHD approximation **(see e.g. [40, 41])**. The scales between $k\ell \sim 10^{-6}$ and $kd_i = 1$ are most likely described by Hall-MHD physics, and the generalized helicity [24] would likely be better conserved at these scales. This, however, requires a computation of vorticity using multi-spacecraft methods,**and is left for a future study**.

The same panel shows the normalized residual energy spectrum for the magnetosheath case. $\sigma_r \sim 0$ at large scales, hinting at near-equipartition of energy between flow and magnetic energies. It decreases approaching smaller scales, indicating a loss in flow energy and dominance of magnetic energy at kinetic scales. Once again, a good agreement with single-spacecraft and multi-spacecraft values is observed. This hints at a difference between magnetosheath and solar wind cases, as will be discussed below.

The bottom panel of this figure shows the alignment angle as a function of scale. At large scales, it has a value ~ -0.4, indicating a degree of anti-alignment. Approaching kinetic scales, $\cos(\theta)$ approaches zero, indicating a lack of (anti-)alignment. This behavior is also seen for the solar wind intervals that we analyzed.

We turn now to discussion of the spectral features of the selected solar wind interval. Spectra of magnetic field, proton flow and electron flow (not shown) display typical features, e.g. power-law spectra, increasing kurtosis at smaller scales etc.; see Ref [38] for details, including issues of cleaning FPI moments in the solar wind. Here we directly move to the study of the equivalent spectrum of cross helicity (shown in figure 3). The vertical

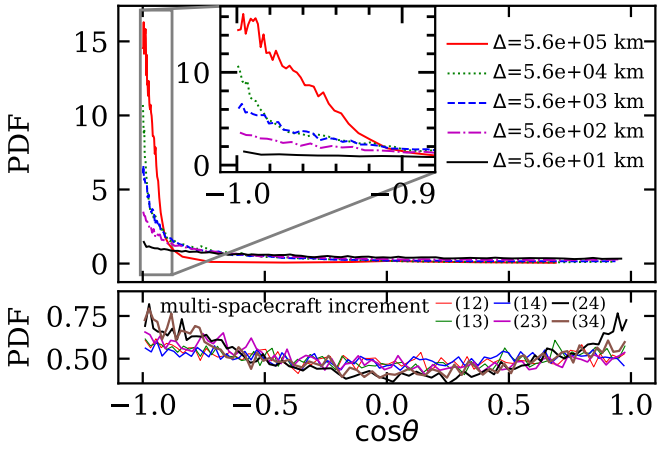

FIG. 4: Solar wind interval: PDFs of alignment angles for various increment lags (top panel) as well as multi-spacecraft lags (bottom panel) with number pairs representing pairs of spacecraft.

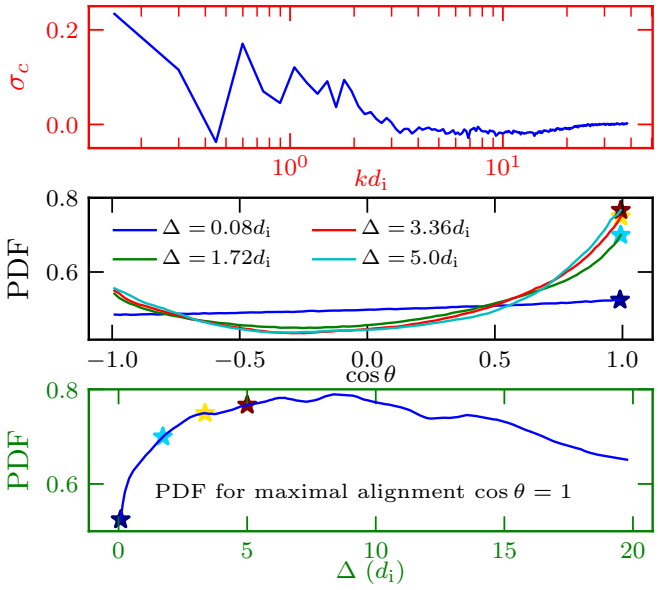

FIG. 5: Cross helicity spectrum, alignment PDFs for small increments, and probability density at maximal alignment (stars in middle panel) as a function of lag for the PIC simulation of [47]. See text for details.

green dash-dotted line shows the low-pass scale for the data cleaning procedure [38]. The light blue cross helicity curve extending beyond the low-pass cutoff is the "Fourier interpolated" data, obtained at the original time cadence after imposing the low-pass filter. Although the results at these scales show a trend similar to figure 2, the results in this range are of questionable validity.

The cross helicity in figure 3 remains close to -0.7 in the inertial range. As kinetic scales are approached, the cross helicity approaches zero, as was seen in the magnetosheath case. However, because the data at these scales is interpolated, this conclusion is qualitative at best. Nevertheless, this interpretation is further supported by multi-spacecraft measurements of σ_c, that are seen also to be close to zero. The overall qualitative picture is similar to what was observed in the magnetosheath, supporting the idea that the trends seen here are not an artifact of sampling, noise, or the data cleaning procedure.

The residual energy for the solar wind interval, also shown in Figure 3, is magnetically dominated at large scales with a value ~ -0.6, and, moving towards proton scales, it approaches equipartition. It is interesting that the multi-spacecraft estimates, deep in the sub-proton kinetic range, have values approaching $\sim 1.$, indicating a preponderance of fluctuation flow energy compared to magnetic energy. The alignment angle spectrum shown in bottom panel of figure 3 also supports the "isotropization" conclusion. Evidently the multi-spacecraft data indicate that magnetic and velocity field have little or no preference to be aligned at the 10 km scale, deep in the kinetic range.

Alignment can be further studied by examination of the probability distribution functions (PDFs) of alignment angles, shown in figure 4. The top panel shows PDFs of $\cos(\theta)$ obtained from increments, from single spacecraft measurements and for lags ranging from 1 to 10000 points ($\equiv 56$ km to 5.6×10^5 km), that is, from sub-proton scales to several correlation scales. The bottom panel shows PDFs for $\delta\mathbf{v}$, $\delta\mathbf{b}$ alignment cosines computed from multi-spacecraft lags, corresponding to kinetic scale measurements. The inset shows a magnification of the initial part of the PDFs. In this particular interval the alignment PDFs peak at $\cos(\theta) = -1$, consistent with $\sigma_c = -0.7$ at large scales. However, a counter-intuitive result is that decreasing the lag decreases the alignment probability even in the inertial range. Once kinetic scales are approached, the alignment is essentially absent, consistent with demagnetization of the protons. Multi-spacecraft PDFs show very slight departures from isotropy. However, the values are close to 0.5 and the PDFs can be treated as almost isotropic.

Discussion: We have presented an analysis of proton velocity and magnetic field fluctuation correlations, alignment and partitioning of energy, studying the transition from MHD to kinetic scales. Such studies are enabled in the MMS mission by the unique combination of high time-cadence and small inter-spacecraft separation, in both magnetosheath and solar wind.

Our main observational results, for the selected intervals, are as follows: • The normalized *cross helicity* σ_c tends towards zero for decreasing scale approaching proton kinetic scales. This has been anticipated in theory [42], but is not always manifest in observations [43] nor realized even in MHD for varying types of turbulence (e.g., [44]). Spacecraft observations of σ_c in the kinetic range have not been previously reported. • **Behavior of σ_r in SW inertial range is qualitatively consistent with MHD theories [45] in that it is magnet-**

ically dominated and approaches isotropy as kinetic scales are approached. The MS case is only partially consistent in the sense that it is magnetically dominated but does not show a tendency towards equipartition. The kinetic range behavior is very different in both cases, indicating a significant departure from MHD behavior. • The (**v**, **b**) **alignment vanishes towards kinetic scales and into the kinetic range. This is a general phenomenon that we have observed in all the MMS intervals that we have analyzed, mainly slow wind, and one fast wind interval (not shown). More fast wind intervals are needed to confirm if this effect prevails in fast wind as well. These findings are** inconsistent with MHD simulation [19] and MHD theory [25]. **Hints of this departure can be seen in some existing studies [26, 43, 46] as the end of inertial range is approached.** Evidently it is a purely kinetic plasma physics phenomenon, deserving of further theoretical study.

Simulation. To further support and elucidate these, we present an analysis from a fully kinetic 3D PIC simulation [47]. The simulation was done on 2048^3 grid points, with $L = 42.$ d_i, $\beta_i = \beta_e = 0.5$, with $\sim 2.6 \times 10^{12}$ particles, and an initial cross helicity of ~ 0.44. The analysis is performed on a snapshot late in time-evolution of the simulation. For more details, refer to [47]. Figure 5 shows the corresponding simulation results for cross helicity, alignment, and residual energy, to be compared with the main observational results above. The Figure shows that σ_c approaches zero in the kinetic range, consistent with the observations. The PDFs of $\cos(\theta)$ show decreasing probability of pure alignment approaching proton kinetic scales. In the bottom panel we also plot the probability of maximal alignment (stars in middle panel) as a function of lag. The probability of maximal alignment increases with decreasing lag initially, consistent with MHD theories [22, 23, 25]. However, at around 10 d_i, the maximal probability begins to drop, indicating increasing frequency of non-aligned proton flow and magnetic field at smaller scales.

These results strengthen the idea that the alignment dynamics are much richer in the kinetic range than they are in inertial range dominated by MHD. The MMS instrument suite opens the doors for these and other novel space plasma studies by providing high-resolution plasma measurements in the kinetic range. Data sets with varied parameters and of longer durations are needed to start exploring some of these counter intuitive and "non-MHD" results. **Observational examination of generalizations of cross helicity in the kinetic range, and of related properties in Hall MHD, EMHD, and other models would require challenging manipulations of the MMS data, and may not be feasible at present. It would be useful to employ a combination of observations and simulations to study these in the future.**

Acknowledgments

This study was supported in part by NASA by the MMS T&M project under grant NNX14AC39G, by LWS program under grant NNX15AB88G, by the Heliophysics Guest Investigator program under grant NNX17AB79G, by NASA grant NNX17AI25G, and by NSF SHINE program under grant AGS-1460130. The authors would like to thank three anonymous referees for their valuable comments that have improved the manuscript significantly.

[1] P. J. Coleman, Jr., The Astrophysical Journal **153**, 371 (1968).
[2] J. W. Belcher and L. Davis Jr., J. Geophys. Res. **76**, 3534 (1971).
[3] C. Tu and E. Marsch, Space Science Reviews **73**, 1 (1995).
[4] R. Bruno and V. Carbone, Living Reviews in Solar Physics **10** (2013), URL `http://www.livingreviews.org/lrsp-2013-2`.
[5] C. Chen, S. Bale, C. Salem, and B. Maruca, The Astrophysical Journal **770**, 125 (2013).
[6] R. T. Wicks, A. Mallet, T. S. Horbury, C. H. Chen, A. A. Schekochihin, and J. J. Mitchell, Physical review letters **110**, 025003 (2013).
[7] C. H. K. Chen, Journal of Plasma Physics **82**, 535820602 (2016).
[8] A. Pouquet, U. Frisch, and J. Lorat, Journal of Fluid Mechanics **77**, 321354 (1976).
[9] W. H. Matthaeus and Y. Zhou, Physics of Fluids B: Plasma Physics **1**, 1929 (1989), https://doi.org/10.1063/1.859110, URL `https://doi.org/10.1063/1.859110`.
[10] A. Yoshizawa and N. Yokoi, The Astrophysical Journal **407**, 540 (1993).
[11] B. Chandran, The Astrophysical Journal **685**, 646 (2008).
[12] B. D. G. Chandran, E. Quataert, G. G. Howes, J. V. Hollweg, and W. Dorland, The Astrophysical Journal **701**, 652 (2009), URL `http://stacks.iop.org/0004-637X/701/i=1/a=652`.
[13] J. C. Perez and S. Boldyrev, Physical review letters **102**, 025003 (2009).
[14] J. Podesta and A. Bhattacharjee, The Astrophysical Journal **718**, 1151 (2010).
[15] W. Matthaeus and M. Goldstein, Journal of Geophysical Research **87**, 6011 (1982), ISSN 0148-0227.
[16] S. Chandrasekhar, Proceedings of the National Academy of Science **42**, 273 (1956).
[17] L. Woltjer, Proc. Nat. Acad. Sci. USA **44**, 833 (1958).
[18] A. C. Ting, W. H. Matthaeus, and D. Montgomery, Physics of Fluids **29**, 3261 (1986).
[19] T. Stribling and W. H. Matthaeus, Physics of Fluids B **3**, 1848 (1991).
[20] D. Telloni, V. Carbone, S. Perri, R. Bruno, F. Lepreti,

and P. Veltri, The Astrophysical Journal **826**, 205 (2016).
[21] L. J. Milano, W. H. Matthaeus, P. Dmitruk, and D. C. Montgomery, Physics of Plasmas **8**, 2673 (2001).
[22] J. Mason, F. Cattaneo, and S. Boldyrev, Phys. Rev. Lett. **97**, 255002 (2006), URL http://link.aps.org/doi/10.1103/PhysRevLett.97.255002.
[23] W. Matthaeus, A. Pouquet, P. Mininni, P. Dmitruk, and B. Breech, Physical review letters **100**, 085003 (2008).
[24] S. Servidio, W. H. Matthaeus, and V. Carbone, Physics of Plasmas **15**, 042314 (2008).
[25] S. Boldyrev, Physical review letters **96**, 115002 (2006).
[26] J. Podesta, B. D. Chandran, A. Bhattacharjee, D. Roberts, and M. Goldstein, Journal of Geophysical Research: Space Physics **114** (2009).
[27] G. Zimbardo, A. Greco, L. Sorriso-Valvo, S. Perri, Z. Vörös, G. Aburjania, K. Chargazia, and O. Alexandrova, Space science reviews **156**, 89 (2010).
[28] W. Matthaeus and M. Velli, Space science reviews **160**, 145 (2011).
[29] L. Turner, IEEE Trans. Plasma Sci. **PS14**, 849 (1986).
[30] H. M. Abdelhamid, M. Lingam, and S. M. Mahajan, The Astrophysical Journal **829**, 87 (2016).
[31] T. Passot, P. Sulem, and E. Tassi, Physics of Plasmas **25**, 042107 (2018).
[32] S. Galtier and R. Meyrand, Journal of Plasma Physics **81** (2015).
[33] D. Telloni and R. Bruno, Monthly Notices of the Royal Astronomical Society: Letters **463**, L79 (2016), URL http://dx.doi.org/10.1093/mnrasl/slw135.
[34] J. L. Burch, R. B. Torbert, T. D. Phan, L.-J. Chen, T. E. Moore, R. E. Ergun, J. P. Eastwood, D. J. Gershman, P. A. Cassak, M. R. Argall, et al., Science **352** (2016), ISSN 0036-8075, http://science.sciencemag.org/content/352/6290/aaf2939.full.pdf, URL http://science.sciencemag.org/content/352/6290/aaf2939.
[35] J. L. Burch, T. E. Moore, R. B. Torbert, and B. L. Giles, Space Science Reviews **199**, 5 (2016), ISSN 1572-9672, URL https://doi.org/10.1007/s11214-015-0164-9.
[36] C. T. Russell, B. J. Anderson, W. Baumjohann, K. R. Bromund, D. Dearborn, D. Fischer, G. Le, H. K. Leinweber, D. Leneman, W. Magnes, et al., Space Science Reviews **199**, 189 (2016), ISSN 1572-9672, URL https://doi.org/10.1007/s11214-014-0057-3.
[37] C. Pollock, T. Moore, A. Jacques, J. Burch, U. Gliese, Y. Saito, T. Omoto, L. Avanov, A. Barrie, V. Coffey, et al., Space Science Reviews **199**, 331 (2016), ISSN 1572-9672, URL https://doi.org/10.1007/s11214-016-0245-4.
[38] R. Bandyopadhyay, A. Chasapis, R. Chhiber, T. Parashar, B. Maruca, W. Matthaeus, S. Schwartz, S. Eriksson, O. LeContel, H. Breuillard, et al., arXiv preprint arXiv:1807.06140 (2018).
[39] A. Chasapis, W. H. Matthaeus, T. N. Parashar, S. A. Fuselier, B. A. Maruca, T. D. Phan, J. L. Burch, T. E. Moore, C. J. Pollock, D. J. Gershman, et al., The Astrophysical Journal Letters **844**, L9 (2017), URL http://stacks.iop.org/2041-8205/844/i=1/a=L9.
[40] T. N. Parashar, W. H. Matthaeus, M. A. Shay, and M. Wan, The Astrophysical Journal **811**, 112 (2015), URL http://stacks.iop.org/0004-637X/811/i=2/a=112.
[41] Y. Voitenko and J. De Keyser, The Astrophysical Journal Letters **832**, L20 (2016).
[42] R. Grappin, A. Pouquet, and J. Léorat, Astron. Astrophys. **126**, 51 (1983).
[43] C.-Y. Tu, E. Marsch, and H. Rosenbauer, Geophys. Res. Lett. **17**, 283 (1990).
[44] W. H. Matthaeus, M. L. Goldstein, and D. C. Montgomery, Phys. Rev. Lett. **51**, 1484 (1983).
[45] R. Grappin, W.-C. Müller, and A. Verdini, Astronomy & Astrophysics **589**, A131 (2016).
[46] A. Verdini, R. Grappin, O. Alexandrova, and S. Lion, The Astrophysical Journal **853**, 85 (2018).
[47] V. Roytershteyn, H. Karimabadi, and A. Roberts, Phil. Trans. R. Soc. A **373**, 20140151 (2015).